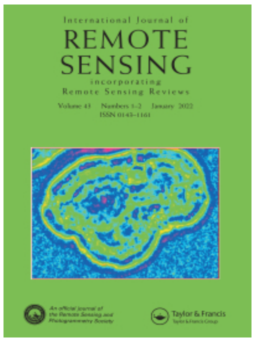

International Journal of Remote Sensing

ISSN: (Print) (Online) Journal homepage: https://www.tandfonline.com/loi/tres20

Dual hybrid convolutional generative adversarial network for hyperspectral image classification

Cuiping Shi, Tianyu Zhang, Diling Liao, Zhan Jin & Liguo Wang

INTERNATIONAL JOURNAL OF REMOTE SENSING
2022, VOL. 43, NO. 14, 5452–5479
https://doi.org/10.1080/01431161.2022.2135412

Dual hybrid convolutional generative adversarial network for hyperspectral image classification

Cuiping Shi[a], Tianyu Zhang[a], Diling Liao[a], Zhan Jin[a] and Liguo Wang[b]

[a]College of Electronic and Communication Engineering, Qiqihar University, Qiqihar, China; [b]College of Information and Communication Engineering, Dalian Nationalities University, Dalian, China

ABSTRACT

Generative adversarial networks (GANs) have effectively promoted the development of hyperspectral image classification technology in generating samples. Many GAN-based models for hyperspectral image classification use deconvolution to generate fake samples, which will cause chequerboard artefacts and affect classification performance. Furthermore, the training of GANs still faces the problem of mode collapse. Aiming at the above problems, we proposed a dual hybrid convolutional generative adversarial network (DHCGAN) for hyperspectral image classification. Firstly, the combination of nearest neighbour upsampling and sub-pixel convolution is employed in the generator, which avoids the overlap of convolution domain and effectively suppresses the chequerboard artefacts caused by deconvolution. Secondly, the traditional convolution and dilated convolution are fused in the discriminator, which expands the receptive field without increasing parameters and achieves more effective feature extraction. In addition, some adaptive drop blocks are embedded into the generator and discriminator to effectively alleviate the problem of mode collapse. Experiments were performed on four hyperspectral datasets (including three classical datasets – Indian Pines, University of Pavia and Houston, a new dataset – WHU-Hi-HanChuan). Experimental results show that the proposed method can provide a certain performance improvement over some competing methods, such as the accuracy has been increased by more than 1% on the three classical datasets, and even got over 3% improvement on WHU_Hi_HanChaun dataset.

ARTICLE HISTORY
Received 19 April 2022
Accepted 9 October 2022

KEYWORDS
hyperspectral image (HSI) classification; generative adversarial network (GAN); sub-pixel convolution; hybrid convolution

1. Introduction

With the development of imaging technology, the development of hyperspectral sensors has become more and more mature, so the processing of hyperspectral images (HSIs) has received extensive attention from researches. HSI processing technology includes many aspects, such as classification, spectral unmixing (Shi and Wang 2014), super-resolution restoration (Jiang et al. 2020) and anomaly detection (Nasrabadi 2014). Classification is one of the most commonly used and critical techniques. HSIs have the characteristics of multiple bands, with hundreds of continuous and narrow spectral bands, covering the

CONTACT Cuiping Shi shicuiping@qqhru.edu.com College of Electronic and Communication Engineering, Qiqihar University, No. 42, Wenhua Street, Jianhua District, Qiqihar 161000, Heilongjiang Province, China

entire range of visible to infrared spectral range, and containing rich spatial and spectral information. Therefore, they have been widely used in agricultural crop analysis (Gu et al. 2017), urbanization analysis (Benediktsson, Palmason, and Sveinsson 2005), environmental pollution monitoring (Arellano et al. 2015), military (Makki et al. 2017) and other fields.

Traditional machine learning classification methods usually include two separate steps, namely, effective feature extraction and classifier design. Due to the huge amount of HSI data, some dimensionality reduction methods have emerged. Their purpose is to convert the original high-dimensional attribute space into low-dimensional subspace data and still achieve the classification effect without dimensionality reduction. The existing dimensionality reduction methods of HSIs mainly include transformation-based methods and non-transformation-based methods. Transformation-based methods include principal component analysis (PCA) (Licciardi et al. 2012), wavelet transform (Bruce, Cliff, and Li 2002). The dimensionality reduction methods based on non-transformation include band selection (Warner and Shank 1997), data source division, etc. Later, some spatial spectral feature extraction methods were proposed (Zhu et al. 2018; Liang et al. 2017; Fang et al. 2018; He et al. 2019). Representative hyperspectral image classifiers include logistic regression (Khodadadzadeh et al. 2014), K-nearest neighbour (Cariou and Chehdi 2015), support vector machine (Melgani and Bruzzone 2004) and limit learning machine (Li et al. 2015), etc. However, the classification effect of the above traditional machine learning methods is not satisfactory, and the extracted features are relatively limited.

Over the past decade, in fields such as computer vision and natural language processing, deep learning has been shown to extract features with strong discriminative power (Ronneberger, Fischer, and Brox 2015; Wang, Li, and Ling 2018). At the same time, deep learning also shows great advantages in HSI classification tasks. For example, in (Chen et al. 2014), a stacked autoencoder for HSI classification was first proposed to obtain more advanced features. Later, variants of SAE (including Laplace SAE (Jia et al. 2015), etc.) had also been proposed one after another. Moreover, Chen et al. proposed a deep belief network model for HSI classification task to realize feature extraction and classification (Chen, Zhao, and Jia 2015). However, these two deep learning frameworks have the problem of over parameterization. Convolutional neural network (CNN) has the characteristics of local connection and parameter sharing, which can effectively alleviate this problem. In addition, many studies have proved that CNN performs well in HSI classification tasks with its powerful automatic feature extraction ability. Hu et al. proposed a one-dimensional CNN (1DCNN) for HSI classification (Hu et al. 2015). Li et al. (2017) proposed a new pixel pair method, which used 1DCNN to classify pixel pairs. Cao et al. (2018) used Markov random field and CNN to learn feature distribution, which can make better use of spatial information. The proposal of the spectral spatial residual network enabled the model to continuously learn the distinguishing features in spectral and spatial, and the classification performance was further improved (Zhong et al. 2018). Then, Zhang, Li, and Du (2018) proposed a new region-based model of learning context interaction information. The deformable idea was introduced, deformable down sampling and deformable convolution were used to achieve effective feature extraction (Zhu et al. 2018). Besides, Jiang et al. (2021) proposed a full convolution spatial propagation network to enhance the modelling of context spatial information.

Except CNN, generative adversarial network (GAN) has also become a widely concerned deep learning model in recent years after it was first proposed (Goodfellow et al.

2014). Because of its ability to generate high-quality samples, it has attracted great attention of many researchers. GAN consists of two sub-networks, the generator and the discriminator. The two sub-networks are trained against each other, not only ensures that the generator provides high-quality samples, but also enables the discriminator to obtain higher discrimination ability. This process also makes its training optimization have some challenges. In the early days, conditional GAN (Mirza and Osindero 2014) could guide the generator to synthesize fake samples of the target. Laplace GAN (Denton, Chintala, and Fergus et al. 2015) utilized the GAN framework to train individual CNN, but its calculation is too complicated. Radford et al. proposed deep convolution GAN (Radford, Metz, and Chintala 2015), successfully integrated CNN into GAN for the first time, and introduced some optimization methods to help GAN stabilize training. There is also a semi-supervised GAN, which uses a small amount of labelled data and a large amount of unlabelled data for GAN training to realize the classification of unlabelled data. Afterwards, some GAN models that can make the training more stable have emerged, such as Wasserstein GAN (Martin, Chintala, and Bottou 2017), progressive growth GAN (Karras et al. 2018), etc.

Due to the high cost of acquiring HSI data, in the case of small samples, GAN can achieve data augmentation by generating samples to effectively alleviate this problem. In the past three years, many researchers have studied GAN adversarial training for HSI classification. For example, Zhan et al. (2018) proposed a one dimensional SGAN framework for HSI classification. And the three dimensional GAN is proposed to combine spatial information and use softmax to assist classification in the discriminator (Zhu et al. 2018). Zhong et al. (2020) proposed a GAN framework combined with conditional random field to reconstruct the real HSI data distribution to alleviate the shortage of training samples. A one-dimensional triple GAN and integrated capsule network was proposed for sample generation (Wang et al. 2019). In addition, Feng et al. (2019) proposed a new multi-class spatial spectral GAN method to complete adversarial training. Recently, Hang et al. (2021) proposed multi-task GAN, designed a generator that undertakes two tasks for reconstruction of the HSI cube and final classification. Zhang et al. (2021) put forward a combined GAN by using the ideas of (Martin, Chintala, and Bottou 2017) and (Karras et al. 2018) for HSI classification. A method of embedding adaptive drop blocks into GAN (ADGAN) was proposed to alleviate the problem of mode collapse during training (Wang et al. 2021). Roy et al. (2022) also used GAN to oversample the minority classes in HSI to alleviate the class imbalance problem in HSI datasets.

However, for many GAN-based HSI classification methods, the network layers of the generator use deconvolution to generate fake samples, but if the parameters of deconvolution are not set properly, it will face chequerboard artefacts. This effect is particularly obvious at the darker borders, which will have a certain impact on the classification performance. Sun et al. introduced sub-pixel convolution into the generator to achieve compressive sensing reconstruction (Sun et al. 2020). Inspired by this, and in order to solve the problem of chequerboard artefacts and mode collapse, a new GAN model-dual hybrid convolution GAN (DHCGAN) is proposed in this paper. In the generator of DHCGAN, the combination of nearest neighbour upsampling and sub-pixel convolution is employed to generate high-quality fake samples as one input of the discriminator. Due to the slow convergence speed of GAN, in order to avoid increasing the computational complexity by setting too many network layers, the dilated convolution is introduced into the discriminator, which integrates the traditional convolution and dilated convolution to achieve more effective feature extraction. Furthermore, the adaptive drop layers and the batch normalization layers were embedded into the generator and discriminator to achieve GAN optimization. It is worth noting that the proposed discriminator has only one output, which can avoid the contradiction between classification and discrimination. In conclusion, the contributions of this paper can be summarized as the following three points.

(1) To our knowledge, we are the first to use this method to provide ideas for sample generation from hyperspectral images, which is a way to use mixed sub-pixel convolutions as upsampling layers on the generator of a GAN.
(2) In the generator, the nearest neighbour upsampling and sub-pixel convolution are effectively combined, which not only suppresses chequerboard artefacts caused by deconvolution, but also generates high-quality samples to alleviate the problem of small sample size of HSI data.
(3) For the discriminator, we fuse the dilated convolution with the traditional convolution, and set different dilation rates for different convolution layers. In generally, the dilation rate increases, which can expand the receptive field and enhance the discriminative ability of the discriminator.

The rest of this paper is arranged as follows. Section 2 briefly reviews the traditional GAN and auxiliary classifier GAN. Section 3 introduces the proposed DHCGAN method in detail. The experimental results and analysis are given in Section 4. Section 5 draws some conclusions.

2. Related works

2.1. Generative adversarial network

GAN is a training image synthesis model based on the idea of game theory. GAN contains two network models, one is generator G and the other is discriminator D. The basic framework of GAN is shown in Figure 1. As shown in Figure 1, the generator G receives a random noise z, which is a n-dimensional vector, and takes the output data $X_{fake} = G(z)$ with the same distribution p_{data} as the real data. The input of discriminator D are real data X_{real} and false data X_{fake} generated by G, and the output is a probability value $P(S|X) = D(X)$. In the training process of GAN, the generator G and discriminator D have contradictory goals.

The goal of G is to learn the distribution of real data, reduce the gap between real data X_{real} and generated data X_{fake}, and try to make D discrimination error. The goal of D is to distinguish real data from generated data as accurately as possible. The optimization process of GAN is to find the Nash equilibrium between G and D, which can be regarded as a minimax game problem. The objective function can be defined as

$$\min_G \max_D V(D,G) = \mathbf{E}_{X_{real}\sim p_{data}}[\log D(X_{real})] + \mathbf{E}_{X_{fake}\sim p_G}[\log(1 - D(X_{fake}))] \tag{1}$$

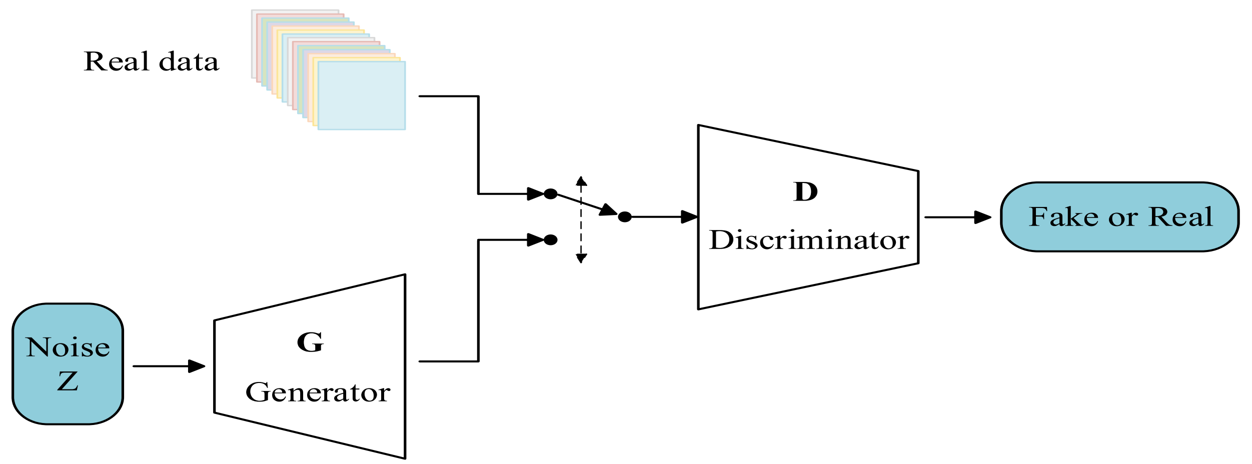

Figure 1. The basic framework of GAN.

Where $V(\cdot)$ and E represent the observed value and the expected operator respectively. In the iteration, first, when G is fixed, the discriminator D is trained and optimized k times to maximize its log-likelihood, and the loss function L_D can be represented as

$$L_D = \mathbf{E}[\log P(S = real|X_{real})] + \mathbf{E}[\log P(S = fake|X_{fake})] \tag{2}$$

Then, when D is fixed, the generator G realizes optimization by minimization L_G, and the loss function L_G can be represented as

$$L_G = \mathbf{E}[\log P(S = fake|X_{fake})] \tag{3}$$

Such confrontation training makes G and D promote each other. After multiple alternating iterative training, the global optimal performance is achieved, that is, the generator G learns the distribution of real data, and the ability of discriminator D to distinguish real data from generated data has also been well improved.

2.2. Auxiliary classifier generative adversarial network

Both conditional GAN (CGAN) and auxiliary classifier GAN (ACGAN) control the generated image by introducing additional conditions. ACGAN is a good proof that adding more structures and a special cost function to the latent space of GAN can obtain higher quality samples (Odena, Olah, and Shlens 2017). The network layers of CGAN are the full connection layer, and the network layers of ACGAN are the convolution layer. The convolution layer can better extract the features of the image, and the generated image edges are more continuous and more realistic. Moreover, the discriminator of ACGAN can output the probability of multi-class labels, which is more suitable for multi-class applications such as HSIs. In ACGAN, each generated sample is assigned an associated class label $c : p_c$, class label c and random noise z are used as the input of generator G and output as labelled false data $X_{fake} = G(c, z)$. Similarly to GAN, the input of discriminator D is the real data with corresponding labels and the fake data with corresponding labels generated by G, and the output is two items: one is the probability distribution

$P(S|X)$ to distinguish real and fake data, and the other is the probability distribution $P(C|X) = D(X)$ to classify the input according to class label c. The objective function of ACGAN has two parts: the log-likelihood of the correct source L_S and the log-likelihood of the correct class L_C. The calculation equations of L_S and L_C can be represented as

$$L_S = \mathbf{E}[\log P(S = real|X_{real})] + \mathbf{E}[\log P(S = fake|X_{fake})] \tag{4}$$

$$L_C = \mathbf{E}[\log P(C = c|X_{real})] + \mathbf{E}[\log P(C = c|X_{fake})] \tag{5}$$

Among them, maximizing $L_S + L_C$ through alternating iterative training can realize the optimization of D, and maximizing $L_C - L_S$ can realize the optimization of G. This paper improved the idea of ACGAN, and proposed the DHCGAN method, and explored the performance of the proposed method in the application of hyperspectral classification.

3. Methodology

3.1. The overall framework of the proposed DHCGAN model

The overall framework of the proposed DHCGAN method is shown in Figure 2. Let $\mathbf{S} = \{\mathbf{X}, \mathbf{Y}\}$ be the input of the model, where $\mathbf{X} \in \Re^{H\times W\times B}$ is a three-dimensional HSI cube with height H, width W, spectral channel B. And $\mathbf{Y}$ is the label vector of HSI data. Because there is a lot of redundancy between the spectral bands of HSI, it is difficult to train a robust generator. Therefore, firstly, PCA is used to concentrate the spectral bands of the input HSI to the first three components, thereby reducing the computational complexity of data processing and contribute to the training and optimization of GAN. The dimension reduced data is randomly divided into blocks, and the three-dimensional cube composed of the target pixel and its spatial neighbourhood pixels is taken as a new sample set

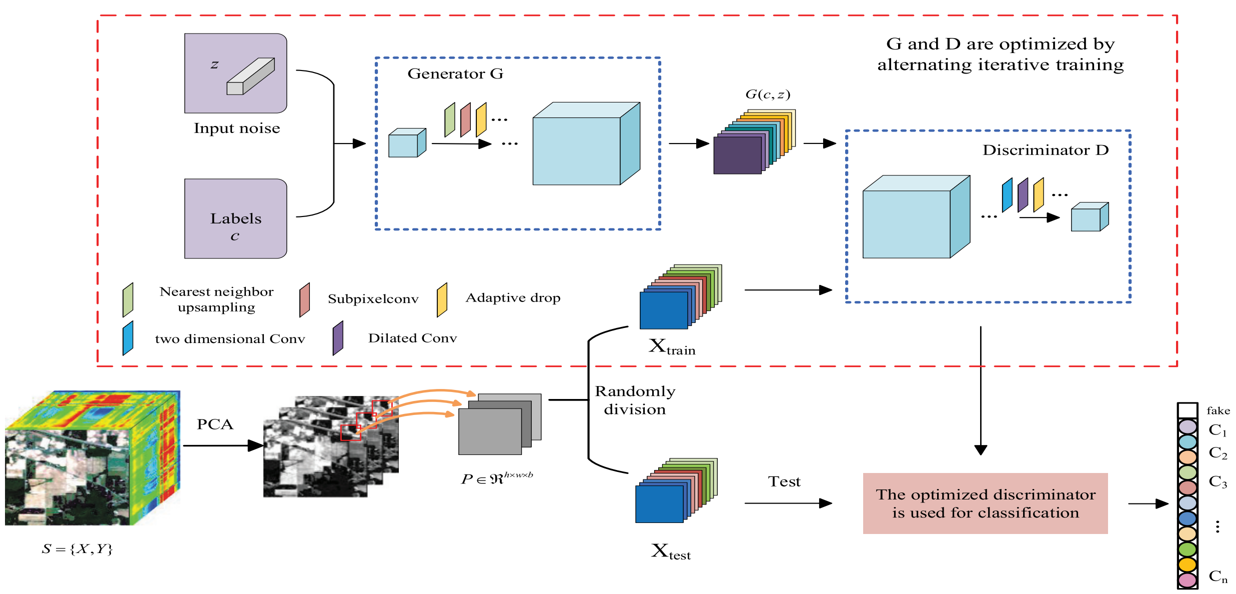

Figure 2. The overall framework of the proposed DHCGAN method.

$\mathbf{P} \in \Re^{h\times w\times b}$, where H and W are set to the same value, representing the height and width of the cube respectively, and B is the number of spectral components obtained by PCA. Next, P is randomly divided into training set x_{train} and test set x_{test} according to a certain proportion.

Generator g and discriminator D are trained alternately to promote and optimize each other. In one iteration, the generator G is trained and optimized once, while the discriminator D is trained and optimized k times. Under the condition of fixed the generator G, the real training sample set x_{train} and some fake samples $G(c, z)$ are input into discriminator D to obtain an output – specific category or fake label. After several iterations, the optimized G and D are obtained. Finally, the test set is input into the optimized discriminator D to get the final classification prediction result.

3.2. Generator with hybrid convolution

Most hyperspectral image classification methods based on GAN model take deconvolution as the main network layer of the generator, but if the parameters are not configured properly, the generated samples are easy to appear obvious chequerboard artefacts. This paper explored the mitigation of chequerboard artefacts in HSI classification task by the combination of nearest neighbour upsampling and sub-pixel convolution. Firstly, the input noise of G is $100 \times 1 \times 1$, and then the input is converted to $512 \times 4 \times 4$ through a nearest neighbour upsampling layer and a conventional two-dimensional convolution layer, where the parameter *upscale* of the nearest neighbour upsampling is set to 4. Then, four combination functions $CF(\cdot)$ are used to further improve the resolution of the tensor obtained above. Specifically, $CF(\cdot)$ is a combined function of sub-pixel convolution, batch normalization (BN) (Ioffe and Szegedy 2015) and activation function Exponential Linear Units (ELU) (Clevert, Unterthiner, and Hochreiter 2016), and the resulting high-resolution output is

$$\mathbf{F_{out}} = CF(x^l) = \sigma[BN_{\alpha,\beta}SubPixel(x^l)] \tag{6}$$

Where, x^l is the input tensor of the lth layer, σ represents the ELU activation function operation, α and β represent the trainable parameters of BN operation respectively, and $SubPixel(\cdot)$ is the sub-pixel convolution operation. If the input tensor size is $[n, In\_C, h, w]$ and the parameter of sub-pixel convolution is r_1, the output size through sub-pixel convolution operation is $[n, \frac{In\_C}{{r_1}^2}, h \times r_1, w \times r_1]$, where n represents the batch size and In_C is the input channels. The parameter settings of each layer of generator G are shown in Table 1. In particular, the adaptive drop layer is set after every two sub-pixel convolution and used twice. The principle of adaptive drop is elaborated in Section 3.4. The final output size of generator G is $3 \times 64 \times 64$.

3.3. Discriminator with hybrid convolution

The dilated convolution is introduced into the discriminator to increase the receptive field of the convolution, so as to improve the discrimination ability of the discriminator. The implementation of discriminator D is listed in Table 2. As shown in Table 2, the discriminator consists of seven layers, including five convolution layers, one adaptive drop layer

Table 1. The implementation details of generator G.

Generator G					
Layer Type	K_Size	Upscale/r_1	Stride	BN?	Activation
Upsampling	–	4	–	no	–
Conv2d	4×4×512	–	2	yes	ELU
Subpixelconv	–	2	1/2	yes	ELU
Subpixelconv	–	2	1/2	yes	ELU
Adaptivedrop	–	–	–	–	–
Subpixelconv	–	2	1/2	yes	ELU
Subpixelconv	–	2	1/2	yes	ELU
Adaptivedrop	–	–	–	–	–
Conv2d	1×1×3	–	1	no	tanh

Table 2. The implementation details of discriminator D.

Discriminator D					
Layer Type	K_Size	Stride	Dilation rate	Padding?	BN?
Conv2d	4×4×64	2	1	yes	no
Conv2d	4×4×128	2	2	yes	yes
Conv2d	4×4×256	2	3	yes	yes
Conv2d	4×4×512	2	4	yes	yes
Adaptivedrop	–	–	–	–	–
Conv2d	4×4×128	1	1	no	no
linear	1×128	–	–	–	–

and one linear layer. The convolution layer has four parameters: convolution kernel size, stride, dilation rate and padding. Set the input feature map size to $[n, In\_C, h, w]$ and the convolution kernel size to $[N, FH, FW]$, where N represents the number of convolution kernels, the stride is s, the padding is p, and the dilation rate is r, which represents the interval of convolution kernels. When $r = 1$, it is standard convolution; and when $r > 1$, it is dilated convolution, and the convolution kernel size of dilated convolution is $[N, DH, DW]$, which can be expressed as

$$DH = r * (FH - 1) + 1 \tag{7}$$

$$DW = r * (FW - 1) + 1 \tag{8}$$

The size of output feature map is

$$OH = \frac{h+2p - [r * (FH - 1) + 1]}{s} + 1 \tag{9}$$

$$OW = \frac{w + 2p - [r * (FW - 1) + 1]}{s} + 1 \tag{10}$$

If multiple identical dilated convolutions are superimposed, a large number of holes will appear, which will lose the continuity and integrity between data and is not conducive to efficient learning. Therefore, we fuse the dilated convolution with the traditional convolution, that is, for a group of dilated convolutions in discriminator D, different layers set different dilation rates (the first four layers are 1,2,3,4 respectively), and the dilation rate increases gradually. This not only ensures that the last layer has a larger receptive field, but also avoids a large loss of local information.

3.4. Adaptive drop block

As a deep neural network, GAN may be over fitted due to excessive parameterization during iterative training optimization, and will also face the problem of mode collapse of the generator. Therefore, BN and an adaptive drop layer are used as regularization methods to alleviate the above problems in this paper. BN has been widely used in deep neural network training. It uses the mean and standard deviation in a mini-batch to continuously adjust the intermediate output of the neural network, so that the value of the intermediate output of the whole neural network in each layer is more stable.

In particular, the adaptive drop method is a structured regularization method with the thought of attention. The schematic figure of dropout (Srivastava et al. 2014) operation is shown in Figure 3, and the schematic figure of adaptive drop method is shown in Figure 3. Among them, the area with valid information is marked with blue square, and the drop operation is marked with black circle. As can be seen from Figure 3, the dropout operation randomly drops pixels with a certain probability in all regions, obviously without using spatial infor mation. Before performing the adaptive drop operation, the current feature map $\mathbf{D}(t)$ is first normalized to obtain the input feature map $\mathbf{A}(t)$. Secondly, a set of pixels of each feature map is sampled using Bernoulli distribution (the yellow circles in Figure 3 are marked as the sampled elements). For the position $\mathbf{M}_{i,j}$ of each element, create a spatial block with size $block\_size \times block\_size$ centred on $\mathbf{M}_{i,j}$. Then the kth percentile element is dropped, the number of features dropped are controlled by γ, and the remaining elements are retained and set to 1. In this way, an adaptive mask with irregular shape is formed. The parameter can be calculated as

$$\gamma = \frac{1 - keep\_prob}{block\_size^2} \frac{{size_{feature\_map}}^2}{\left(size_{feature\_map} - block\_size + 1\right)^2} \tag{11}$$

Where, $keep\_prob$ is the same as that in dropout operation, which is set between 0.75 and 0.95, and $size_{feature\_map}$ represents the size of the feature map for performing the adaptive drop operation.

Finally, apply the resulting adaptive mask, the output is

$$\mathbf{A}^{(t+1)} = \mathbf{A}^{t} \times count(\mathbf{M})/count\_ones(\mathbf{M}) \tag{12}$$

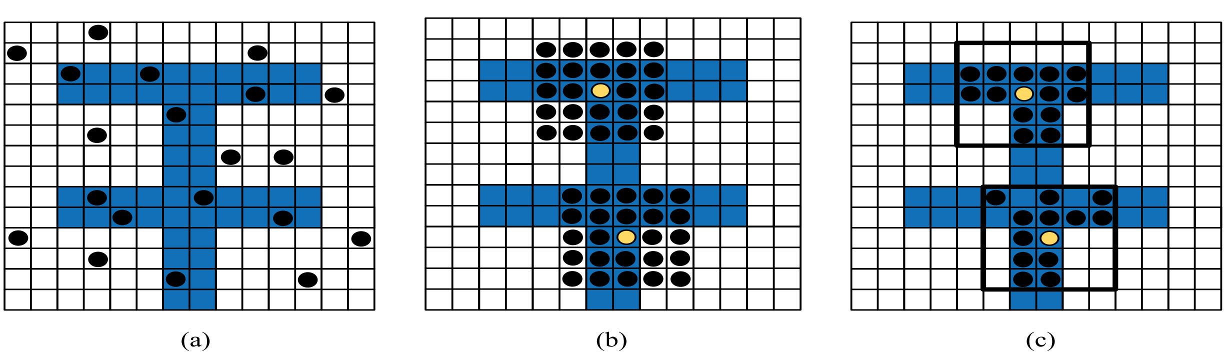

Figure 3. The schematic of (a) dropout; (b)(c) adaptive drop.

Where, $count(\mathbf{M})$ indicates the number of elements in the mask, and $count\_ones(\mathbf{M})$ indicates that the number of elements in the mask is 1.

3.5. Training and optimization of DHCGAN

As mentioned above, the training between generator and discriminator is performed as a two-player minimax game, which can be represented as

$$\min_{G}\max_{D} V(D,G) = E_{x\sim p_{data}(x)}[\log D(x)] + E_{z\sim p_{G}(z)}[\log(1 - D(G(z)))] \tag{13}$$

The goal of discriminator D is to maximize Equation (12) , while the goal of the generator is to fool discriminator, that is, to minimize Equation (12). Obviously, when $p_G(Z) = p_{data}(x)$, G is optimal. The procedure of the proposed DHCGAN method is shown in Algorithm 1.

Algorithm The procedure of the proposed DHCGAN method

Input: Training sample x_{train} and test sample x_{test}, one hot label c of training sample, batch size n, number E of training epochs, noise dimension d, update optimization times k of discriminator

```
Initialization: All weight matrices and offsets for G and D
for E training iterations do
  for k times do
    Input the training sample x_train with three spectral components to D to complete the training of real samples;
    Randomly generated d-dimensional noisez;
    Generate fake samples G(c, z) with one hot labels by generator G with hybrid convolution;
    Input the fake sample to D to obtain the classification result;
    Update the parameters of D by maximizing V(D, G) by Equation (12);
  end
  Input random noise z into G to generate fake samples G(c, z);
  Update the parameters of G by minimizing V(D, G) by Equation (12);
end
```

Output: Final specific category $c = \{c_i\}_{i=1}^{n}$ or false label of test sample x_{test}

4. Experimental results and analysis

4.1. Hyperspectral data sets

1) *Indian Pines*: The Indian Pine dataset was obtained from the Airborne Visible Infrared Imaging Spectrometer sensor in northwest Indiana. Figure 4 shows the pseudocolor and the corresponding ground truth image of the Indian Pines dataset. The spatial resolution is 20 m per pixel and the spectral coverage is 0.4 2.5 μm. The data size is 145×145. After eliminating the 20 bands (include 104–108, 150–163 and 200) that cannot be reflected by water, the remaining 200 effective bands are taken as the research object. There are 16 land cover categories.

2) *University of Pavia*: The University of Pavia dataset was collected by Reflective Optics System Imaging Spectrometer sensors. The spectral coverage range is 0.43 0.86 μm, with a total of 115 bands, and the spatial resolution is 1.3 m. The data size is 610×340. After removing the noise influence band, there are 103 effective bands left for research, with a total of 9 kinds of crops. Figure 5 shows the pseudocolor and the corresponding ground truth image of the University of Pavia dataset.

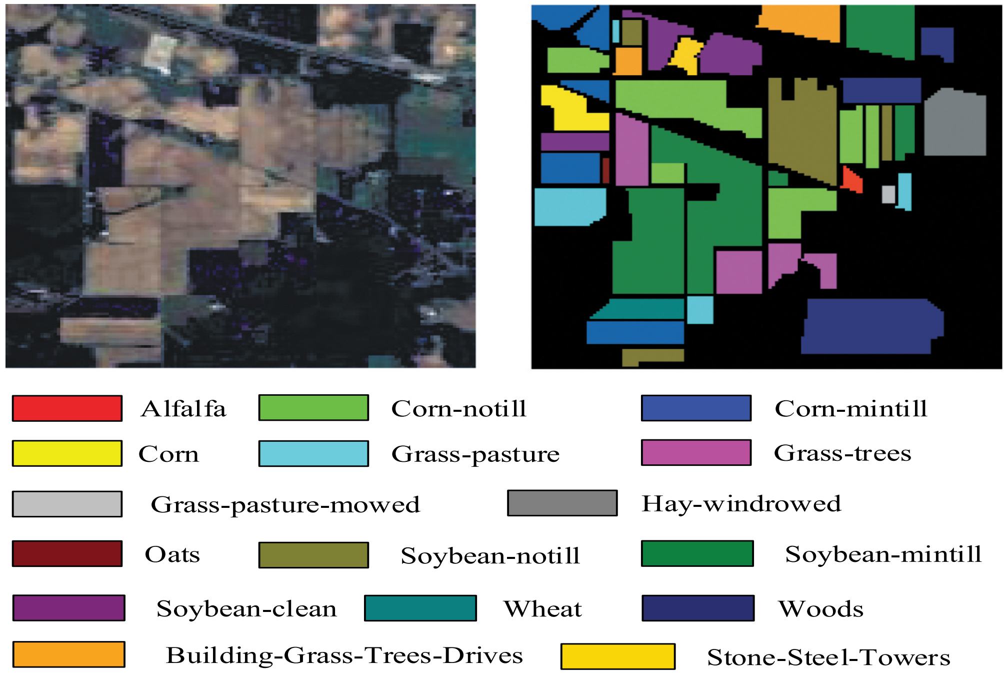

Figure 4. The pseudocolor and the corresponding ground truth image of the Indian Pines dataset.

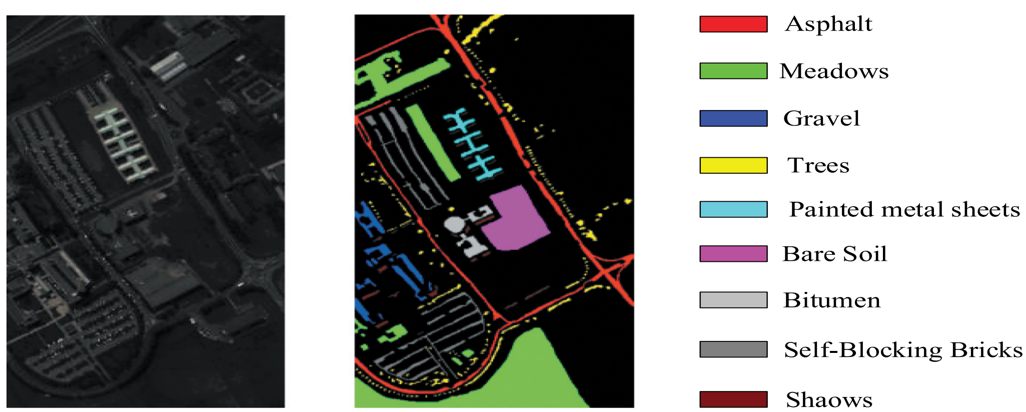

Figure 5. The pseudocolor and the corresponding ground truth image of the University of Pavia dataset.

3) *WHU-Hi-HanChuan*: The WHU-Hi-HanChuan dataset was acquired on 17 June 2016, in Hanchuan, Hubei province, China, with an 17-mm focal length Headwall Nano-Hyperspec imaging sensor equipped on a Leica Aibot X6 Unmanned Aerial Vehicle (UAV) V1 platform. The image size is 1217×303, there are 274 bands in the range of 400–1000 nm, and the spatial resolution is about 0.109 m/pixel. There are 16 types of land cover. Figure 6 shows the pseudocolor and the corresponding ground truth image of WHU-Hi-HanChuan dataset.

Figure 6. The pseudocolor and the corresponding ground truth image of the WHU-Hi-HanChuan dataset.

Figure 7. The pseudocolor and the corresponding ground truth image of the Houston dataset.

4) *Houston*: This dataset was collected by the NSF-funded Center for Airborne Laser Mapping over the University of Houston campus and the neighbouring urban area. The size of the scene is $349 \times 1905 \times 144$ with a spatial resolution 2.5 m/pixel and spectral coverage ranging from 0.38 to 1.05 μm. Fifteen land-cover classes were contained. Figure 7 shows the pseudocolor and the corresponding ground truth image of Houston dataset.

4.2. Evaluation index and parameter setting

In this paper, three commonly used quantitative measurement methods, including overall classification accuracy (OA), average classification accuracy (AA), and statistical kappa coefficient (kappa), are used to evaluate the performance of the proposed DHCGAN. The proportion of correctly classified samples in the total number of test samples is denoted by OA. The average of classification accuracy was determined as AA. Kappa represents the consistency between the classification map and the ground truth map, and the lower its value, the worse the classification effect. In the experiment, the batch size of each dataset is set to 200, and the input spatial window size is 27×27. In addition, the weight initialization of the proposed DHCGAN is random. Adam is used to optimize the parameters of the model. The initial learning rate is set to 0.0002, and the input random noise vector of the generator is set to 100 dimensions. All experimental results were obtained by independently running more than 20 times. Tables 3–6 show the number of

Table 3. Number of training and test samples per class in the Indian pines dataset.

Class		Numbers of samples	
No	Name	Train	Test
1	Alfafa	5	41
2	Corn-notill	139	1289
3	Corn-mintill	81	749
4	Corn	23	214
5	Grass-pasture	47	436
6	Grass-trees	71	659
7	Grass-pasture-mowed	3	25
8	Hay-windrowed	46	432
9	Oats	2	18
10	Soybean-notill	95	877
11	Soybean-mintill	240	2215
12	Soybean-clean	58	535
13	Wheat	20	185
14	Woods	123	1142
15	Building-grass-trees-drives	38	348
16	Stone-steal-towers	9	84
	Total	1000	9249

Table 4. Number of training and test samples per class in the University of Pavia dataset.

Class		Numbers of samples	
No	Name	Train	Test
1	Asphalt	155	6476
2	Meadows	436	18213
3	Gravel	49	2050
4	Trees	72	2992
5	Painted metal sheets	31	1314
6	Bare Soil	118	4911
7	Bitumen	31	1299
8	Self-Blocking Bricks	86	3596
9	Shadows	22	925
	Total	1000	41776

training and test samples per class of the proposed DHCGAN on Indian pines, University of Pavia, WHU-Hi-HanChuan and Houston datasets. The computer device used for the experiment consists of an Intel i9-9900k processor with 128 GB of memory and NVIDIA GeForce RTX 2080 Ti GPU.

4.3. Classification results and analysis

To verify the effectiveness of the proposed DHCGAN, this paper makes comparative experiments with some state-of-the-art classification methods (including random forest (RF) (Ham et al. 2005), support vector machine (SVM) with radial basis function, multilayer perceptron (MLP) (Collobert and Bengio 2004), three-dimensional CNN (3DCNN) (Chen et al. 2016), pyramidal residual networks (PyResNet) (Paoletti et al. 2019), ADGAN, SpectralFormer (Hong et al. 2022), graph convolutional networks (GCN) (Hong et al. 2021)). Both RF and SVM belong to traditional machine learning methods, and MLP is a feedforward neural network with two full connection layers. 3DCNN and PyResNet

Table 5. Number of training and test samples per class in the WHU-Hi-HanChuan dataset.

Class		Numbers of samples	
No	Name	Train	Test
1	Strawberry	69	44710
2	Cowpea	35	22728
3	Soybean	15	10262
4	Sorghum	9	5328
5	Water spinach	2	1175
6	Watermelon	7	4508
7	Greens	9	5878
8	Trees	28	17953
9	Grass	15	9444
10	Red roof	17	10491
11	Grey roof	27	16886
12	Plastic	6	3654
13	Bare soil	14	9091
14	Road	28	18535
15	Bright object	2	1111
16	Water	117	75376
	Total	400	257130

Table 6. Number of training and test samples per class in the Houston dataset.

Class		Numbers of samples	
No	Name	Train	Test
1	Healthy grass	65	1186
2	Stressed grass	65	1189
3	Synthetic grass	40	657
4	Trees	65	1179
5	Soil	65	1177
6	Water	20	305
7	Residential	66	1202
8	Commercial	65	1179
9	Road	65	1187
10	Highway	64	1163
11	Railway	64	1171
12	Parking Lot 1	64	1169
13	Parking Lot 2	30	439
14	Tennis Court	25	403
15	Running Track	38	623
	Total	800	14229

belong to the CNN model of deep learning, while ADGAN and DHCGAN belong to the GAN-based classification algorithm in the deep learning framework. Obviously SpectralFormer and GCN are based on Transformer and graph convolutional network frameworks, respectively. In the RF method, the maximum features number of split nodes is set to 20, and 200 trees are constructed for each dataset before taking the average prediction. For CNN models (3DCNN and PyResNet), the input image patch size is set to 11×11, at which point their classification performance is the best. The input image patch size of ADGAN is set to the size for best performance, which is 27×27. PyResNet, ADGAN, SpectralFormer, GCN and the proposed DHCGAN are implemented under the framework of Pytorch, and the other four algorithms are experimented in the framework of Keras. The

Table 7. Classification results of different methods on Indian pines dataset.

Color	Class	RF	SVM	MLP	3DCNN	PyResNet	ADGAN	SpectralFormer	GCN	DHCGAN
	1	19.00	0.00	35.17	28.89	83.13	96.30	97.41	94.44	**98.83**
	2	54.90	70.44	62.79	81.16	92.75	96.35	85.33	87.94	**96.40**
	3	46.57	87.48	68.52	88.7	87.02	95.52	80.24	86.98	**96.81**
	4	16.00	11.69	52.79	70.43	83.48	**96.89**	95.23	79.24	96.81
	5	69.28	86.26	86.19	91.68	88.05	93.58	94.37	96.23	**97.00**
	6	74.07	90.47	85.50	95.34	93.42	94.65	90.61	97.30	**99.80**
	7	40.05	10.40	75.54	35.85	94.24	94.03	**97.11**	85.71	94.92
	8	86.25	93.19	89.32	97.48	**100.0**	**100.0**	95.23	97.09	**100.0**
	9	35.10	0.00	59.87	49.37	76.11	82.73	85.89	77.77	**89.84**
	10	47.45	67.87	68.69	84.41	91.98	93.07	87.17	9449	**95.22**
	11	68.12	88.98	69.97	89.04	93.92	94.79	87.43	88.96	**94.33**
	12	29.66	58.79	61.25	60.26	89.84	96.27	91.07	87.32	**98.52**
	13	72.82	97.43	87.18	80.40	92.85	99.98	96.64	97.14	**100.0**
	14	87.37	92.34	89.37	95.96	98.31	97.51	95.87	95.32	**98.91**
	15	26.43	57.22	69.36	83.69	77.83	**95.69**	89.05	82.96	92.75
	16	58.76	94.90	98.61	95.56	91.45.	98.08	95.42	97.72	**98.90**
	OA(%)	69.04	75.45	73.74	86.63	92.80	95.81	88.30	90.07	**96.78**
	AA(%)	51.99	63.31	72.50	76.64	89.65	95.40	91.51	89.79	**96.07**
	Kappa(%)	63.76	71.87	69.79	84.71	91.92	94.81	86.60	88.67	**96.40**

classification results of the seven methods on the four datasets are shown in Table 7–Table 10. The best results are marked in bold.

(1) *Classification results on the Indian pines dataset*: The classification results of the seven algorithms on the Indian pines dataset are shown in Table 8. 500 samples of the Indian pines dataset were randomly selected as training samples and the rest as test samples. It can be seen that the proposed DHCGAN achieved the highest values in OA, AA and kappa, which are 96.78%, 96.07% and 96.40% respectively. Since sophisticated methods based on deep learning (3DCNN, PyResNet, ADGAN, SpectralFormer, GCN and DHCGAN) have more powerful feature extraction

Table 8. Classification results of different methods on University of Pavia dataset.

Color	Class	RF	SVM	MLP	3DCNN	PyResNet	ADGAN	SpectralFormer	GCN	DHCGAN
	1	79.59	88.56	88.74	87.86	95.25	92.59	88.88	93.99	**95.94**
	2	97.55	97.12	98.18	96.07	99.40	98.03	96.80	96.22	**98.44**
	3	64.71	81.19	62.27	85.60	82.64	85.01	69.09	86.45	**86.60**
	4	84.28	86.58	**99.07**	98.90	85.29	97.18	98.91	97.64	94.36
	5	97.85	98.39	99.61	98.82	95.44	**100.0**	99.32	99.91	**100.0**
	6	56.60	85.63	67.01	95.67	94.40	98.01	95.63	93.04	**100.0**
	7	60.54	85.81	83.28	93.14	96.53	96.76	73.72	92.35	**97.21**
	8	83.25	83.92	84.33	78.40	**94.81**	93.33	84.16	86.28	90.70
	9	99.12	99.12	98.78	97.37	77.48	92.11	98.49	**100.0**	99.93
	OA(%)	86.11	91.49	88.87	92.47	95.20	95.10	92.39	94.35	**96.55**
	AA(%)	80.39	89.59	86.81	92.43	91.25	94.78	89.44	93.99	**95.91**
	Kappa(%)	81.17	88.68	85.38	89.94	93.89	95.09	89.88	92.48	**96.24**

abilities, their OA values are superior to traditional machine learning methods (RF and SVM). The network structure of MLP is too simple, so the OA value is lower than that of SVM and other deep learning models. Because SpectralFormer only utilizes spectral information, its accuracy is lower than other algorithms that combine spatial information. For PyResNet, which is also a CNN model, its ability to extract spectral spatial features is stronger than 3DCNN, resulting in three performance indicators that are higher than those of 3DCNN. GCN obtains complex structural information based on the spectral structure of the graph, so the classification performance is better than that of 3DCNN and other algorithms that only utilize spectral information. The classification algorithm based on GAN can effectively alleviate the dilemma of insufficient samples of hyperspectral datasets to a certain extent, so the OA values of ADGAN and DHCGAN are higher than those of other methods. Because the proposed DHCGAN algorithm effectively combines two types of convolution in both generator and discriminator, it not only alleviates chequerboard artefacts caused by deconvolution, but also improves the feature discrimination ability of discriminator, so the three evaluation values are all optimal. Figure 8 are the visual classification maps of different competitive methods on Indian pines dataset. RF, SVM, MLP and 3DCNN presented high misclassification rate on many classes, especially Alfafa, Corn, Oats, Soybean-mintil and Soybean-clean.Moreover, the boundary of the classification maps of these methods is more blurred and the influence of noise is obvious. In contrast, PyResNet, ADGAN and DHCGAN significantly improve the classification quality of each class. Compared with PyResNet, the two GAN models classify more clearly boundaries of each class and have fewer noise points. The proposed DHCGAN achieved the highest accuracy in 13 classes, and the classification effect is particularly significant on the Soybean-notill and Soybean-mintill classes with more samples in the middle region.

(2) *Classification results on the University of Pavia dataset*: In this paper, 1000 samples are randomly selected from the University of Pavia as the training set, and the other samples are used for testing. Table 8 shows the OA, AA and kappa values of

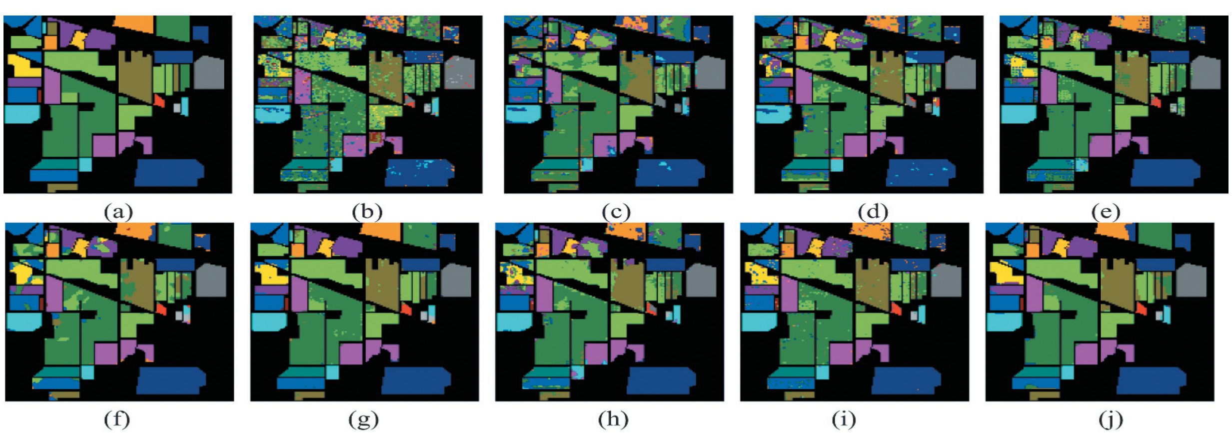

Figure 8. Visual classification maps of different methods on Indian pines dataset (a) the ground truth, (b) RF, (c) SVM, (d) MLP, (e) 3DCNN, (f) PyResnet, (g) ADGAN, (h) SpectralFormer, (i) GCN, (j) DHCGAN.

different competitive methods on the University of Pavia dataset and the classification accuracy of each class. As shown in Table 8, the proposed DHCGAN achieved the highest values in OA, AA and kappa. Among them, the OA values of DHCGAN are 10.44%, 5.06%, 7.68%, 4.08%, 1.35%, 4.16%, 2.2% and 1.45% higher than those of RF, SVM, MLP, 3DCNN, PyResNet, SpectralFormer, GCN and ADGAN respectively. The classification effect of more complex deep learning classification methods (including 3DCNN, PyResNet, ADGAN and DHCGAN) is significantly better than other methods, especially Gravel, Bare Soil and Bitumen. Compared with 3DCNN, the OA value of PyResNet, which is more efficient for feature extraction, is more than 2% higher than 3DCNN. For GAN models, the proposed DHCGAN not only generates high-quality samples, but also extracts features more effectively, so its OA value is higher than PyResNet and ADGAN. The visual classification results corresponding to different competitive methods are shown in Figure 9(b–j). Compared to other methods, DHCGAN achieved the best accuracy on six classes (9 classes in total) of the University of Pavia dataset, and even achieved 100% classification results on Painted metal sheets and Bare Soil.

3) Classification results on the WHU-Hi-HanChuan dataset: Due to the spatial resolution of WHU-Hi-HanChuan data set is very high, the difference between samples of several categories (such as Strawberry, Cowpea, Soybean and Watermelon) is small. Moreover, we

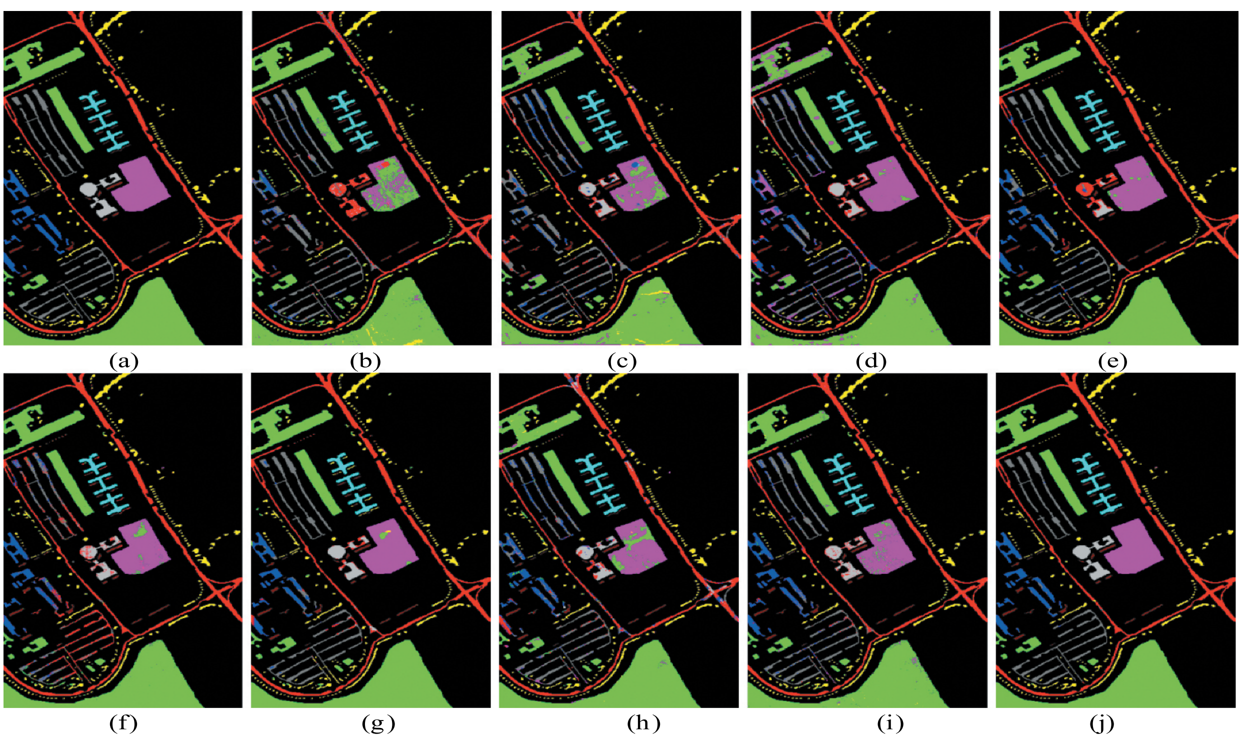

Figure 9. Visual classification maps of different methods on University of Pavia dataset (a) the ground truth, (b) RF, (c) SVM, (d) MLP, (e) 3DCNN, (f) PyResnet, (g) ADGAN, (h) SpectralFormer, (i) GCN, (j) DHCGAN.

Table 9. Classification results of different methods on WHU-Hi-HanChuan dataset.

Color	Class	RF	SVM	MLP	3DCNN	PyResNet	ADGAN	SpectralFormer	GCN	DHCGAN
	1	84.91	77.42	86.87	89.90	68.25	88.05	85.55	85.81	**90.29**
	2	50.57	44.71	70.98	72.01	71.01	73.24	57.98	60.46	**73.95**
	3	17.28	39.67	39.24	60.61	79.54	72.86	60.31	67.03	**80.45**
	4	48.30	60.55	80.64	82.43	77.10	88.97	83.56	83.86	**90.67**
	5	0.0	13.42	19.60	53.51	**55.16**	49.03	12.46	22.56	43.39
	6	0.0	12.37	45.68	46.80	69.05	68.51	20.76	43.42	**71.73**
	7	52.34	51.76	37.28	73.94	71.79	**76.82**	65.24	63.89	64.55
	8	40.19	55.86	76.77	70.05	**87.78**	85.18	67.21	68.67	81.21
	9	0.0	32.19	72.60	56.54	40.74	78.79	54.68	60.14	**79.42**
	10	72.87	83.07	78.93	74.71	86.69	77.90	94.32	**94.59**	88.86
	11	41.31	74.22	76.04	82.05	90.12	87.11	86.10	90.58	**92.50**
	12	0.0	24.07	25.33	54.09	66.04	72.54	43.22	20.99	**73.24**
	13	35.03	40.11	31.14	49.55	36.48	46.51	46.59	49.12	**53.34**
	14	71.18	70.89	63.21	80.20	76.90	79.61	79.30	83.02	**80.90**
	15	66.67	33.57	81.12	71.55	72.50	73.02	**95.95**	86.43	70.25
	16	86.87	95.47	90.12	86.17	81.34	98.64	97.99	96.41	**98.74**
	OA(%)	68.98	70.71	73.08	78.60	81.89	81.34	79.84	81.13	**85.88**
	AA(%)	41.72	50.58	60.97	69.01	70.66	68.67	65.70	67.33	**77.09**
	Kappa(%)	62.89	65.45	68.19	74.59	81.87	78.01	76.33	77.85	**83.46**

randomly selected 400 samples of this dataset as training samples in the experiment, which is equivalent to the training proportion of 0.1%. These are the reasons for the poor accuracy on WHU_Hi_HanChuan dataset. In the case of few training samples, the proposed DHCGAN method also achieves the highest OA, AA and kappa values. As shown in Table 9, compared with ADGAN, DHCGAN 's OA value increased by 4.54%, kappa value increased by 5.45%, and AA value even increased by more than 8%. There are too few samples in several classes in WHU-Hi-HanChuan dataset, resulting in too large differences in classification results between classes. For example, on Water spinach, Watermelon, Grass and Plastic classes, RF is all misclassified. The classification accuracy of other methods in these classes is also less than 80%. However, the proposed DHCGAN achieved the highest value in 11 land-cover categories (16 classes in total), and even achieved the OA value of 98.74% on Water class. Figure 10 shows the classification map visualization results of seven competitive methods on the WHU-Hi-HanChuan dataset. As can be seen from (b), (d), (e) and (g) of Figure 10, the RF, MLP, 3DCNN and ADGAN methods misclassify many samples belonging to Plastic class to Bare Soil class. Compared with them, the classification effect of PyResNet and the proposed DHCGAN on plastic class is better.

4) Classification results on the Houston dataset: For the Houston dataset, 800 samples are randomly selected as the training set, and the other samples are used for testing. Table 10 shows the three evaluation indicators (OA, AA and kappa) and the accuracy of each class with different competitive methods on the Houston dataset. It can be seen from Table 10, the proposed DHCGAN achieved the highest result of OA, AA and kappa. Among them, the OAs of DHCGAN are 4.73%, 3.01%, 5.55%, 1.28%, 0.19%, 1.37%, 5.4% and 1.95% higher than that of the competitive methods respectively. Compared with other methods, DHCGAN achieved the best accuracy on ten classes (15 classes in total) of

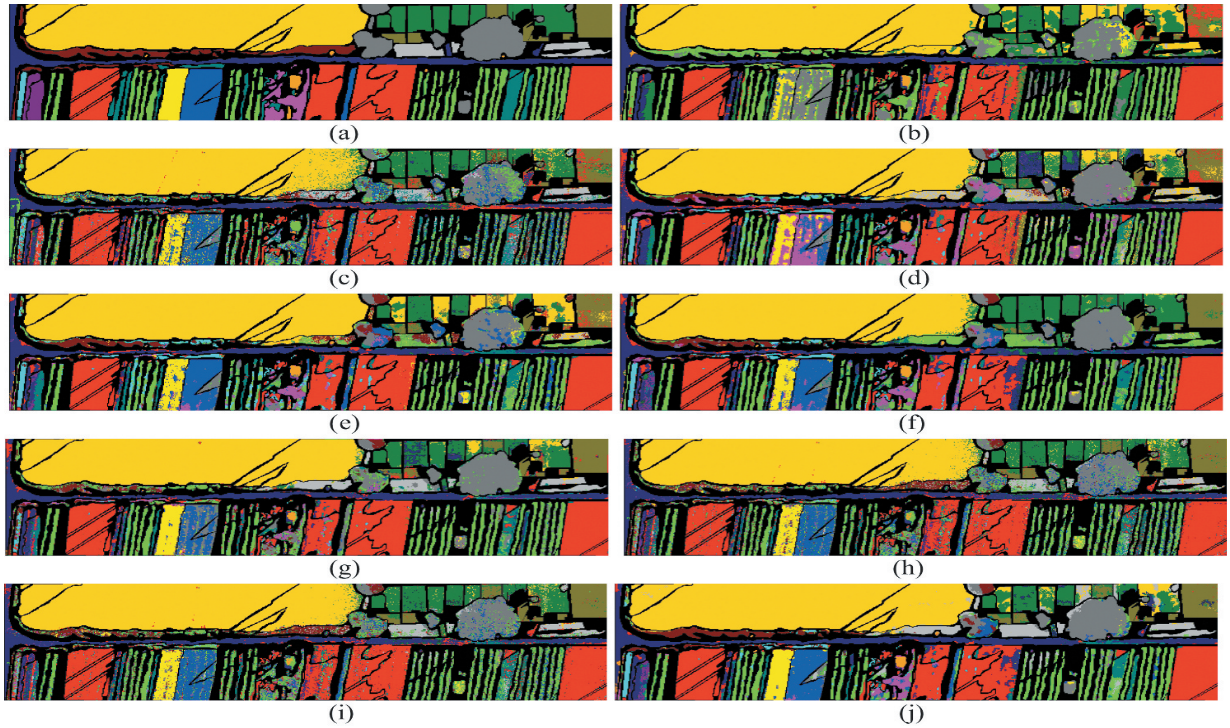

Figure 10. Visual classification maps of different methods on WHU-Hi-HanChuan dataset (a) the ground truth, (b) RF, (c) SVM, (d) MLP, (e) 3DCNN, (f) PyResnet, (g) ADGAN, (h) SpectralFormer, (i) GCN, (j) DHCGAN.

Table 10. Classification results of different methods on Houston dataset.

Color	Class	RF	SVM	MLP	3DCNN	PyResNet	ADGAN	SpectralFormer	GCN	DHCGAN
	1	96.48	95.98	94.32	96.33	95.66	94.96	93.07	97.37	**98.72**
	2	98.24	96.97	97.05	98.09	97.36	87.08	92.07	98.18	**98.64**
	3	99.24	99.56	99.70	99.62	99.80	99.13	94.18	98.62	**100.0**
	4	96.54	97.93	95.53	**98.02**	95.75	91.88	95.56	97.10	94.69
	5	93.07	95.57	91.53	96.64	99.17	96.37	96.00	95.68	**99.91**
	6	90.10	99.53	93.85	99.31	92.04	99.69	87.62	**100.0**	74.30
	7	87.15	88.55	75.90	92.14	**95.75**	80.44	88.98	92.14	81.74
	8	81.20	84.14	83.42	84.88	90.83	**91.07**	80.47	85.30	82.20
	9	88.07	82.55	85.50	85.27	92.22	55.51	84.47	84.72	**97.69**
	10	85.72	86.82	82.53	89.07	89.94	97.63	79.63	90.56	**99.18**
	11	83.63	87.93	86.75	92.89	93.53	93.19	89.1	88.24	**94.57**
	12	80.81	84.28	57.50	86.51	87.63	95.62	82.88	84.38	**98.21**
	13	74.85	76.39	**87.58**	78.57	94.56	77.18	85.90	71.59	72.28
	14	90.47	97.28	99.52	97.31	97.06	**100.0**	91.50	97.77	**100.0**
	15	99.19	99.37	82.92	98.20	98.35	**100.0**	95.02	99.50	**100.0**
	OA(%)	89.21	90.93	88.39	92.66	93.75	92.57	88.54	91.99	**93.94**
	AA(%)	89.71	91.52	88.14	92.86	94.64	91.73	89.10	92.08	**95.05**
	Kappa(%)	88.33	90.19	87.45	92.06	93.46	90.53	87.59	91.34	**96.20**

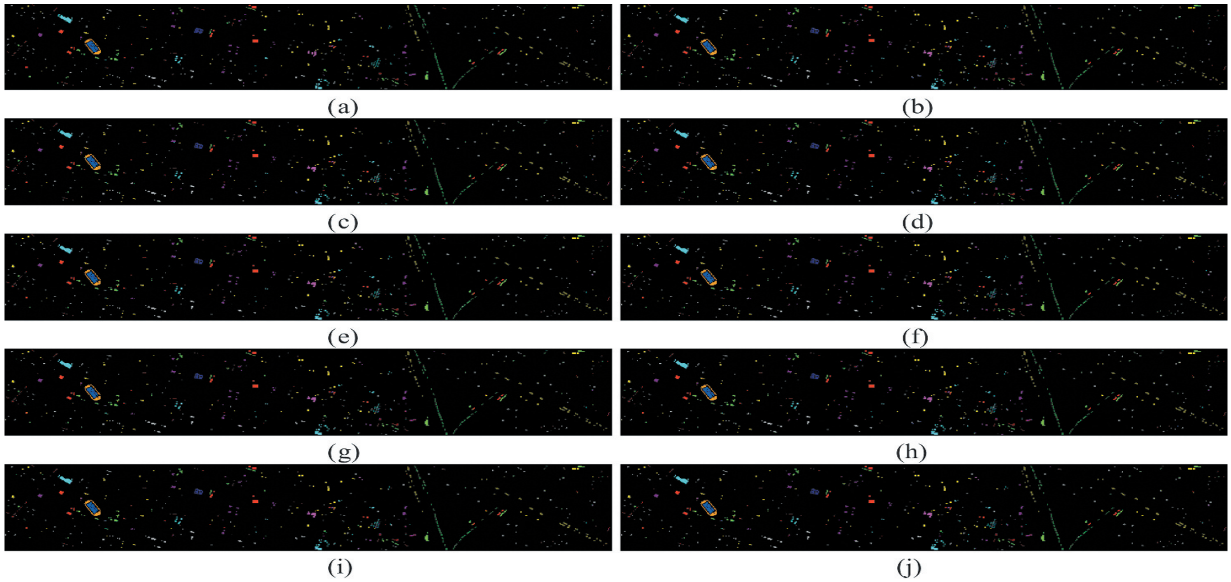

Figure 11. Visual classification maps of different methods on Houston dataset (a) the ground truth, (b) RF, (c) SVM, (d) MLP, (e) 3DCNN, (f) PyResnet, (g) ADGAN, (h) SpectralFormer, (i) GCN, (j) DHCGAN.

the Houston dataset. The OA of PyResNet, which is more efficient for feature extraction, is slightly lower than that of the proposed method, and higher than that of others. For GAN models, the proposed DHCGAN not only generates high-quality samples, but also extracts features more effectively, so its OA is higher than that of PyResNet. The visual classification results of different competitive methods are shown in Figure 11.

4.4. Visualization of generated samples

Table 11 shows the OA values obtained by generators with different convolution strategies on four datasets. The generated samples visualization of different convolution strategies under different training epoch are shown in Figure 12. As can be seen from Table 11, compared with the deconvolution strategy used only in the generator, the strategy combining nearest neighbour upsampling and sub-pixel convolution is 0.5% higher on the four datasets. It can also be seen from Figure 12(a) that during the training process, only using deconvolution presents more or less chequerboard artefacts. The hybrid convolution strategy not only suppresses the chequerboard artefacts, alleviates the overlap of convolution domains, but also improves the classification performance.

Table 11. OA (%) on four datasets with different convolution strategies applied to generator G.

Strategy \ Datasets	Indian Pines	University of Pavia	WHU-Hi-HanChuan	Houston
With hybridconv	96.78	96.55	85.88	93.94
With onlydeconv	96.21	96.09	85.11	91.84

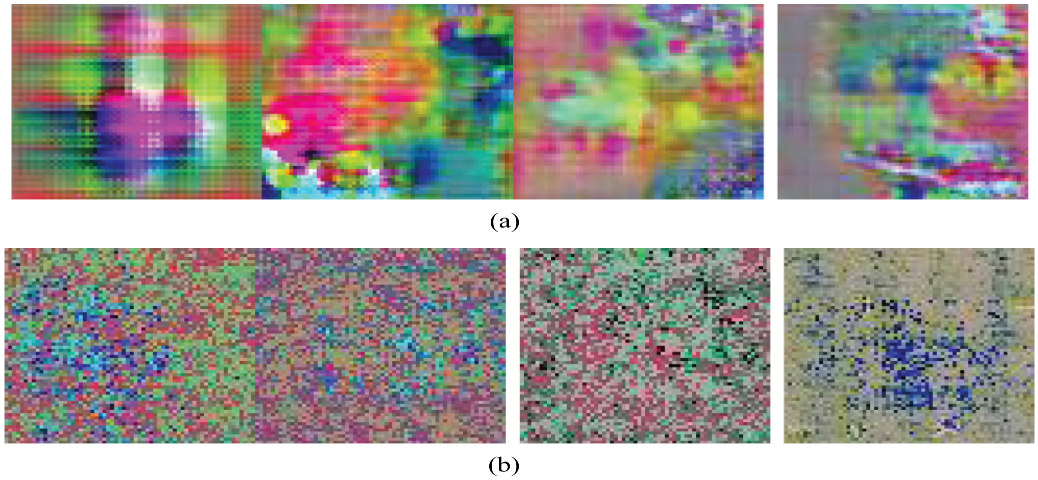

Figure 12. Generated samples visualization of different epochs (from left to right: 200 400 600 800) (a) with only deconv (b) with hybridconv.

4.5. *Efficiency analysis of input image size*

Usually, we classify the target pixel and its spatial neighbours into the same class. Therefore, the patch size of the input image is an important parameter that affects the classification performance. If this value is too small, it may lead to ineffective utilization of spatial information and reduce the classification ability. If it is too large, pixels of different categories may be mixed in the patch area, which is not conducive to the final classification. Figure 13 shows the OA values of four datasets with different input image patch sizes, which are set from 15 to 31 with an interval of 4. As can be seen from Figure 13, with the increase of the input image patch, the OA values obtained on the Indian pins, University of Pavia, Houston and WHU-Hi-HanChuan datasets are also increasing. When

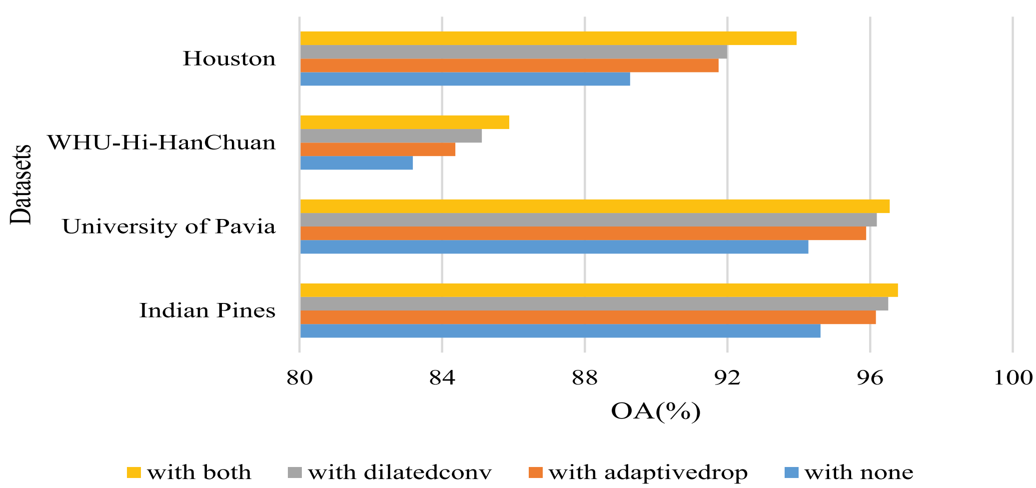

Figure 13. Impact of input image patch size on classification performance.

the input image patch value is 27, the maximum values are obtained, which are 96.78%, 96.55% and 85.88% respectively. Subsequently, the OA value at 31 is slightly lower than that at 27. Therefore, the input image patch size used in this paper is 27, and the proposed method has the best classification performance on each dataset.

4.6. Comparison of running time

In addition to the three commonly used evaluation indicators, running time is also an important index to measure the performance of classification model. Table 12 shows the test time of seven algorithms on four datasets. Due to the complexity of deep learning framework, MLP, 3DCNN, PyResNet, ADGAN, SpectralFormer, GCN and the proposed methods take longer running time than traditional machine learning methods (including RF and SVM). MLP has fewer layers, so its running time is less than other deep learning models. Also based on the CNN model, the PyResNet algorithm has deep network layers and high computational complexity, which causes it to take longer time than the 3DCNN model. GAN-based models (including ADGAN and the proposed DHCGAN) are essentially two sub-networks in alternating iterative training, so they take the longest time. Although the proposed DHCGAN runs long on Indian pines and WHU-Hi-HanChuan datasets, DHCGAN on the four datasets shows the best classification performance.

4.7. Ablation experiment

As previously mentioned, the proposed DHCGAN utilizes adaptive drop layers with attention thought to alleviate the mode collapse problem of GAN. In addition, the dilated convolution is placed in the discriminator, and the feature discrimination ability of the discriminator can be enhanced by setting different dilation rates in different convolution layers. Thus, we did some ablation experiments using a generator with a combination of nearest neighbour upsampling and sub-pixel convolutions and a discriminator containing only traditional convolutions as the basic GAN model. Figure 14 shows the classification accuracy obtained by different strategies on four datasets.

As can be seen from Figure 14, after only the adaptive drop layer is added to the basic model, the OA value of each dataset has a slight increase. Nevertheless, after only replacing a set of dilated convolutions on the basic model, the OA value of each dataset has been greatly improved, indicating that the dilated convolution improves the feature discrimination ability of the discriminator and has an obvious impact on the final classification effect. Obviously, combining the advantages of both (adaptive drop layer and

Table 12. Running time of different methods on four datasets (s).

methods / datasets	RF	SVM	MLP	3DCNN	PyResNet	ADGAN	SpectralFormer	GCN	DHCGAN
Indian pines	4.1	9.4	8.9	65.7	320.3	406.3	55.4	8.9	439.6
University of Pavia	6.8	24.3	15.5	268.1	530.5	518.5	131.1	20.2	500.1
WHU-Hi-HanChuan	62.6	276.6	227.2	1120.9	3643.3	3250.9	1342.0	213.4	3419.3
Houston	10.1	23.6	19.0	96.8	187.9	2386.9	55.9	111.2	2381.3

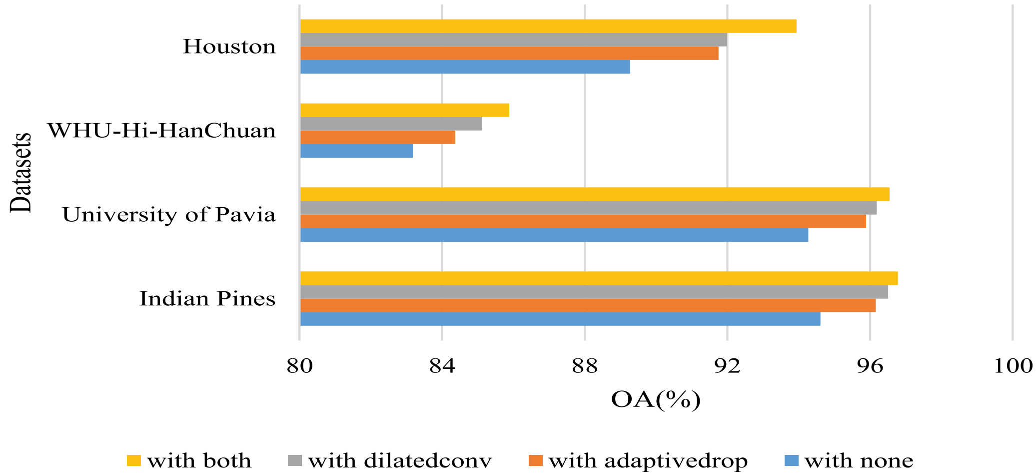

Figure 14. OA (%) of different strategies on four datasets.

dilated convolution), the classification performance of the model composed of the two (i.e. the proposed DHCGAN) is the best.

4.8. Efficiency analysis of the number of training samples

The OA results of the seven methods under different numbers of training samples are shown in Figure 15. In the Indian pines dataset, 300, 500 and 1000 samples were randomly selected for training. For the University of Pavia dataset, 500, 1000 and 2000 samples were randomly selected as training samples. For the WHU-Hi-HanChuan dataset, the number of training samples was randomly set to 200, 400 and 800 respectively. And 450, 800, 1500 samples are randomly selected from the Houston dataset as the training set to verify Experiments indicate that the proposed DHCGAN shows the best performance compared with RF, SVM, MLP, 3DCNN, PyResNet, SpectralFormer, GCN and ADGAN. The framework based on deep learning outperform RF and SVM for classification. With the increase of the number of training samples, the performance of all methods improves, and the proposed DHCGAN obtains higher OA value than other algorithms. Therefore, even under a limited number of training samples, the proposed DHCGAN can show satisfactory and stable performance.

5. Conclusions

In this paper, we propose a novel GAN model for HSI classification – DHCGAN. DHCGAN is divided into two sub-networks. In the generator of DHCGAN, the effective combination of nearest neighbour upsampling and sub-pixel convolution is used to generate high-quality fake samples as an input of the discriminator. Due to the slow convergence speed of GAN, and too many network layers will lead to a large increase in computational complexity. By introducing dilated convolution in the discriminator, and the effective hybrid of

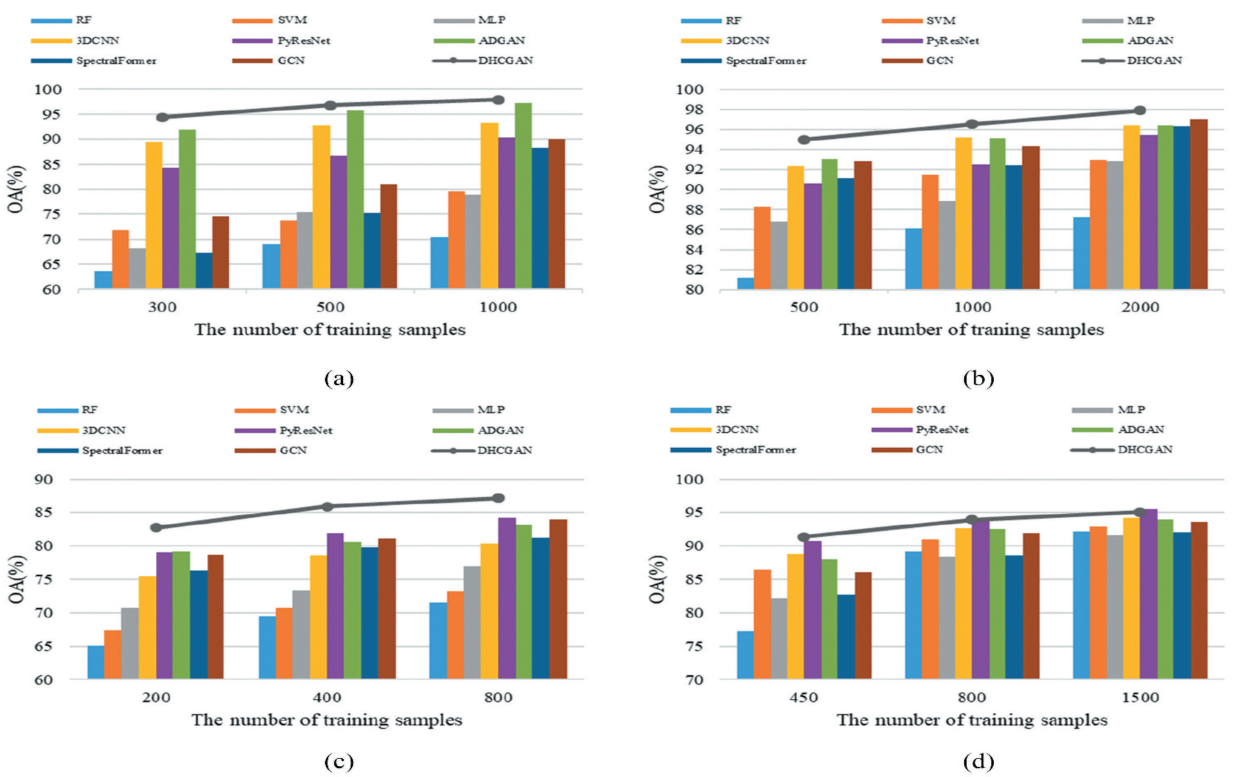

Figure 15. OA (%) of different methods with different numbers of training samples (a) Indian pines, (b) University of Pavia, (c) WHU-Hi-HanChuan, (d) Houston.

traditional convolution and dilated convolution is used to realize more effective feature extraction. In addition, the adaptive drop layer and batch normalization layer are embedded into the generator and discriminator to further optimize GAN. Experiments on four datasets demonstrate that the proposed method outperforms the state-of-the-art GAN model in classification, which proves the effectiveness of DHCGAN.

Acknowledgments

The authors would like to thank the editors and the reviewers for their help and suggestion.

Disclosure statement

No potential conflict of interest was reported by the author(s).

Funding

This research was funded in part by the National Natural Science Foundation of China (42271409, 62071084), in part by the Heilongjiang Science Foundation Project of China under Grant LH2021D022, and in part by the Fundamental Research Funds in Heilongjiang Provincial Universities of China under Grant 135509136.

Data availability statement

The Indiana Pines, University of Pavia, Kennedy Space Center and Salinas Valley datasets are available online at http://www.ehu.eus/ccwintco/index.php?title= Hyperspectral_Remote_Sensing_Scenes (accessed on 3 July 2021). The code of this article is available online at https://github.com/scp19801980/DHCGAN.

References

Arellano, P., K. Tansey, H. Balzter, and D. S. Boyd. 2015. “Detecting the Effects of Hydrocarbon Pollution in the Amazon Forest Using Hyperspectral Satellite Images.” *Environmental Pollution* 205: 225–239. doi:https://doi.org/10.1016/j.envpol.2015.05.041.

Benediktsson, J. A., J. A. Palmason, and J. R. Sveinsson. 2005. “Classification of Hyperspectral Data from Urban Areas Based on Extended Morphological Profiles.” *IEEE Transactions on Geoscience and Remote Sensing* 43 (3): 480–491. doi:http://dx.doi.org/10.1109/TGRS.2004.842478.

Bruce, L. M., H. K. Cliff, and J. Li. 2002. “Dimensionality Reduction of Hyperspectral Data Using Discrete Wavelet Transform Feature Extraction.” *IEEE Transactions on Geoscience and Remote Sensing* 40 (10): 2331–2338. doi:http://dx.doi.org/10.1109/TGRS.2002.804721.

Cao, X., F. Zhou, L. Xu, D. Meng, Z. Xu, and J. Paisley. 2018. “Hyperspectral Image Classification with Markov Random Fields and a Convolutional Neural Network.” *IEEE Transactions on Image Processing* 27 (5): 2354–2367. doi:https://doi.org/10.1109/TIP.2018.2799324.

Cariou, C., and K. Chehdi. 2015. “Unsupervised Nearest Neighbors Clustering with Application to Hyperspectral Images.” *IEEE Journal of Selected Topics in Signal Processing* 9 (6): 1105–1116. doi: https://doi.org/10.1109/JSTSP.2015.2413371 .

Chen, Y., H. Jiang, C. Li, X. Jia, and P. Ghamisi. 2016. “Deep Feature Extraction and Classification of Hyperspectral Images Based on Convolutional Neural Networks.” *IEEE Transactions on Geoscience and Remote Sensing* 54 (10): 6232–6251. doi:https://doi.org/10.1109/TGRS.2016.2584107.

Chen, Y., Z. Lin, X. Zhao, G. Wang, and Y. Gu. 2014. “Deep Learning-Based Classification of Hyperspectral Data.” *IEEE Journal of Selected Topics in Applied Earth Observations and Remote Sensing* 7 (6): 2094–2107. doi:https://doi.org/10.1109/JSTARS.2014.2329330.

Chen, Y., X. Zhao, and X. Jia. 2015. “Spectral–spatial Classification of Hyperspectral Data Based on Deep Belief Network.” *IEEE Journal of Selected Topics in Applied Earth Observations and Remote Sensing* 8 (6): 2381–2392. doi:https://doi.org/10.1109/JSTARS.2015.2388577.

Clevert, D., T. Unterthiner, and S. Hochreiter. 2016. “Fast and Accurate Deep Network Learning by Exponential Linear Units (ELUs).” *arXiv 1511 07289*. doi:https://doi.org/10.48550/arXiv.1511.07289

Collobert, R., and S. Bengio. 2004. “Links Between Perceptrons, MLPs and SVMs.” International conference on Machine learning (ICML) 2004. 10.1145/1015330.1015415.

Denton, E., S. Chintala , A. Szlam, and R. Fergus. 2015. ”Deep Generative Image Models Using a Laplacian Pyramid of Adversarial Networks.” *arXiv 1506*. 05751. https://doi.org/10.48550/arXiv.1506.05751.

Fang, L., N. He, S. Li, P. Ghamisi, and J. A. Benediktsson. 2018. “Extinction Profiles Fusion for Hyperspectral Images Classification.” *IEEE Transactions on Geoscience and Remote Sensing* 56 (3): 1803–1815. doi:https://doi.org/10.1109/TGRS.2017.2768479.

Feng, J., H. Yu, L. Wang, X. Cao, X. Zhang, and L. Jiao. 2019. “Classification of Hyperspectral Images Based on Multiclass Spatial–spectral Generative Adversarial Networks.” *IEEE Transactions on Geoscience and Remote Sensing* 57 (8): 5329–5343. doi:https://doi.org/10.1109/TGRS.2019.2899057 .

Goodfellow, I., J., Pouget-Abadie, M., Mirza, B., Xu, D., Warde-Farley, S., Ozair, A., Courville, and Y., Bengio. 2014. “Generative Adversarial Nets.” International Conference on Neural Information Processing Systems (NIPS) 2014. 2672–2680. https://doi.org/10.48550/arXiv.1406.2661.

Gu, Y., J. Chanussot, X. Jia, and J. A. Benediktsson. 2017. “Multiple Kernel Learning for Hyperspectral Image Classification: A Review.” *IEEE Transactions on Geoscience and Remote Sensing* 55 (11): 6547–6565. doi:https://doi.org/10.1109/TGRS.2017.2729882.

Ham, J., Y. Chen, M. M. Crawford, and J. Ghosh. 2005. "Investigation of the Random Forest Framework for Classification of Hyperspectral Data." *IEEE Transactions on Geoscience and Remote Sensing* 43 (3): 492–501. doi:https://doi.org/10.1109/TGRS.2004.842481.
Hang, R., F. Zhou, Q. Liu, and P. Ghamisi. 2021. "Classification of Hyperspectral Images via Multitask Generative Adversarial Networks." *IEEE Transactions on Geoscience and Remote Sensing* 59 (2): 1424–1436. doi:https://doi.org/10.1109/TGRS.2020.3003341.
He, N., M. E. Paoletti, J. M. Haut, L. Fang, S. Li, A. Plaza, and J. Plaza. 2019. "Feature Extraction with Multiscale Covariance Maps for Hyperspectral Image Classification." *IEEE Transactions on Geoscience and Remote Sensing* 57 (2): 755–769. doi:https://doi.org/10.1109/TGRS.2018.2860464.
Hong, D., L. Gao, J. Yao, B. Zhang, A. Plaza, and J. Chanussot. 2021. "Graph Convolutional Networks for Hyperspectral Image Classification." *IEEE Transactions on Geoscience and Remote Sensing* 59 (7): 5966–5978. doi:https://doi.org/10.1109/TGRS.2020.3015157.
Hong, D., Z. Han, J. Yao, L. Gao, B. Zhang, A. Plaza, and J. Chanussot. 2022. "SpectralFormer: Rethinking Hyperspectral Image Classification with Transformers." *IEEE Transactions on Geoscience and Remote Sensing* 60: 1–15. doi:https://doi.org/10.1109/TGRS.2022.3172371.
Hu, W., Y. Huang, L. Wei, F. Zhang, and H. Li. 2015. "Deep Convolutional Neural Networks for Hyperspectral Image Classification." *Journal of Sensors* 2015: 258619. doi:http://dx.doi.org/10.1155/2015/258619.
Ioffe, S., and C. Szegedy. 2015. "Batch Normalization: Accelerating Deep Network Training by Reducing Internal Covariate Shift." *arXiv 1502* 03167. doi:10.48550/arXiv.1502.03167.
Jiang, Y., Y. Li, S. Zou, H. Zhang, and Y. Bai. 2021. "Hyperspectral Image Classification with Spatial Consistence Using Fully Convolutional Spatial Propagation Network." *IEEE Transactions on Geoscience and Remote Sensing* 59 (12): 10425–10437. doi:https://doi.org/10.1109/TGRS.2021.3049282 .
Jiang, J., H. Sun, X. Liu, and J. Ma. 2020. "Learning Spatial-Spectral Prior for Super-Resolution of Hyperspectral Imagery." *IEEE Transactions on Computational Imaging* 6: 1082–1096. doi:https://doi.org/10.1109/TCI.2020.2996075.
Jia, K., L. Sun, S. Gao, Z. Song, and B. E. Shi. 2015. "Laplacian Auto-Encoders: An Explicit Learning of Nonlinear Data Manifold." *Neurocomputing* 160: 250–260. doi:10.1016/j.neucom.2015.02.023.
Khodadadzadeh, M., J. Li, A. Plaza, and J. M. Bioucas-Dias. 2014. "A Subspace-Based Multinomial Logistic Regression for Hyperspectral Image Classification." *IEEE Geoscience and Remote Sensing Letters* 11 (12): 2105–2109. doi:https://doi.org/10.1109/LGRS.2014.2320258.
Liang, J., J. Zhou, Y. Qian, L. Wen, X. Bai, and Y. Gao. 2017. "On the Sampling Strategy for Evaluation of Spectral-Spatial Methods in Hyperspectral Image Classification." *IEEE Transactions on Geoscience and Remote Sensing* 55 (2): 862–880. doi:https://doi.org/10.1109/TGRS.2016.2616489.
Licciardi, G., P. R. Marpu, J. Chanussot, and J. A. Benediktsson. 2012. "Linear versus Nonlinear PCA for the Classification of Hyperspectral Data Based on the Extended Morphological Profiles." *IEEE Geoscience and Remote Sensing Letters* 9 (3): 447–451. doi:https://doi.org/10.1109/LGRS.2011.2172185 .
Li, W., C. Chen, H. Su, and Q. Du. 2015. "Local Binary Patterns and Extreme Learning Machine for Hyperspectral Imagery Classification." *IEEE Transactions on Geoscience and Remote Sensing* 53 (7): 3681–3693. doi:https://doi.org/10.1109/TGRS.2014.2381602.
Li, W., G. Wu, F. Zhang, and Q. Du. 2017. "Hyperspectral Image Classification Using Deep Pixel-Pair Features." *IEEE Transactions on Geoscience and Remote Sensing* 55 (2): 844–853. doi:https://doi.org/10.1109/TGRS.2016.2616355.
Makki, I., R. Younes, C. Francis, T. Bianchi, and M. Zucchetti. 2017. "A Survey of Landmine Detection Using Hyperspectral Imaging." *ISPRS Journal of Photogrammetry and Remote Sensing* 124: 40–53. doi:https://doi.org/10.1016/j.isprsjprs.2016.12.009.
Martin, A., S. Chintala, and L. Bottou, 2017. Wasserstein Generative Adversarial Networks. International conference on machine learning. PMLR. https://doi.org/10.5555/3305381.3305404.
Melgani, F., and L. Bruzzone. 2004. "Classification of Hyperspectral Remote Sensing Images with Support Vector Machines." *IEEE Transactions on Geoscience and Remote Sensing* 42 (8): 1778–1790. doi:https://doi.org/10.1109/TGRS.2004.831865.

Mirza, M., and S. Osindero. 2014. "Conditional Generative Adversarial Nets." *arXiv 1411 1784*. https://arxiv.org/abs/1411.1784 .

Nasrabadi, N. 2014. "Hyperspectral Target Detection: An Overview of Current and Future Challenges." *IEEE Signal Processing Magazine* 31 (1): 34–44. doi:https://doi.org/10.1109/MSP.2013.2278992.

Odena, A., C. Olah, and J. Shlens. 2017. "Conditional Image Synthesis with Auxiliary Classifier GANs." *Proceedings of the International Conference on Machine Learning. International Conference on Machine Learning* 2642–2651. https://doi.org/abs/1610.09585.

Paoletti, M. E., J. M. Haut, R. Fernandez-Beltran, J. Plaza, A. J. Plaza, and F. Pla. 2019. "Deep Pyramidal Residual Networks for Spectral–spatial Hyperspectral Image Classification." *IEEE Transactions on Geoscience and Remote Sensing* 57 (2): 740–754. doi:https://doi.org/10.1109/TGRS.2018.2860125.

Radford, A., L. Metz, and S. Chintala. 2015. "Unsupervised Representation Learning with Deep Convolutional Generative Adversarial Networks." *arXiv 1511 06434*. doi:10.48550/arXiv.1511.0643.

Ronneberger, O., P. Fischer, and T. Brox, 2015. U-Net: Convolutional Networks for Biomedical Image Segmentation. in MICCAI. https://arxiv.org/abs/1505.04597.

Roy, S. K., J. M. Haut, M. E. Paoletti, S. R. Dubey, and A. Plaza. 2022. "Generative Adversarial Minority Oversampling for Spectral–spatial Hyperspectral Image Classification." *IEEE Transactions on Geoscience and Remote Sensing* 60: 1–15. doi:https://doi.org/10.1109/TGRS.2021.3052048.

Shi, C., and L. Wang. 2014. "Incorporating Spatial Information in Spectral Unmixing: A Review." *Remote Sensing of Environment* 149: 70–87. doi:https://doi.org/10.1016/j.rse.2014.03.034.

Sun, Y., J. Chen, Q. Liu, and G. Liu. 2020. "Learning Image Compressed Sensing with Sub-Pixel Convolutional Generative Adversarial Network." *Pattern Recognition* 98: 98. doi:https://doi.org/10.1016/j.patcog.2019.107051 .

Wang, J., F. Gao, J. Dong, and Q. Du. 2021. "Adaptive DropBlock-Enhanced Generative Adversarial Networks for Hyperspectral Image Classification." *IEEE Transactions on Geoscience and Remote Sensing* 59 (6): 5040–5053. doi:https://doi.org/10.1109/TGRS.2020.3015843.

Wang, R. J., X. Li, and C. X. Ling. 2018. "Pelee: A Real-Time Object Detection System on Mobile Devices." *Neural Information Processing Systems (NIPS)* 1967–1976. https://arxiv.org/abs/1804.06882 .

Wang, X., K. Tan, Q. Du, Y. Chen, and P. Du. 2019. "Caps-TripleGan: GAN-Assisted CapsNet for Hyperspectral Image Classification." *IEEE Transactions on Geoscience and Remote Sensing* 57 (9): 7232–7245. doi:https://doi.org/10.1109/TGRS.2019.2912468.

Warner, T., and M. Shank. 1997. "Spatial Autocorrelation Analysis of Hyperspectral Imagery for Feature Selection." *Remote Sensing of Environment* 60 (1): 58–70. doi:https://doi.org/10.1016/S0034-4257(96)00138-1.

Zhang, F., J. Bai, J. Zhang, Z. Xiao, and C. Pei. 2021. "An Optimized Training Method for GAN-Based Hyperspectral Image Classification." *IEEE Geoscience and Remote Sensing Letters* 18 (10): 1791–1795. doi:https://doi.org/10.1109/LGRS.2020.3009017.

Zhang, M., W. Li, and Q. Du. 2018. "Diverse Region-Based CNN for Hyperspectral Image Classification." *IEEE Transactions on Image Processing* 27 (6): 2623. doi:https://doi.org/10.1109/TIP.2018.2809606.

Zhan, Y., D. Hu, Y. Wang, and X. Yu. 2018. "Semisupervised Hyperspectral Image Classification Based on Generative Adversarial Networks." *IEEE Geoscience and Remote Sensing Letters* 15 (2): 212–216. doi:https://doi.org/10.1109/LGRS.2017.2780890.

Zhong, Z., J. Li, D. A. Clausi, and A. Wong. 2020. "Generative Adversarial Networks and Conditional Random Fields for Hyperspectral Image Classification." *IEEE Transactions on Cybernetics* 50 (7): 3318–3329. doi:https://doi.org/10.1109/TCYB.2019.2915094.

Zhong, Z., J. Li, Z. Luo, and M. Chapman. 2018. "Spectral–spatial Residual Network for Hyperspectral Image Classification: A 3-D Deep Learning Framework." *IEEE Transactions on Geoscience and Remote Sensing* 56 (2): 847–856. doi:https://doi.org/10.1109/TGRS.2017.2755542.

Zhu, J., L. Fang, and P. Ghamisi. 2018. "Deformable Convolutional Neural Networks for Hyperspectral Image Classification." *IEEE Geoscience and Remote Sensing Letters* 15 (8): 1254–1258. doi:https://doi.org/10.1109/LGRS.2018.2830403.

Zhu, J., J. Hu, S. Jia, X. Jia, and Q. Li. 2018. "Multiple 3-D Feature Fusion Framework for Hyperspectral Image Classification." *IEEE Transactions on Geoscience and Remote Sensing* 56 (4): 1873–1886. doi: https://doi.org/10.1109/TGRS.2017.2769113.

报告编号：**L24N2022-3094**

检 索 报 告

一、检索要求

1. 委 托 人：石翠萍(Shi, CP (Shi, Cuiping))

2. 委托单位：齐齐哈尔大学

3. 检索目的：论文被 SCI-E 收录、所在期刊的影响因子及中国科学院文献情报中心期刊分区表情况

二、检索范围

Science Citation Index Expanded (SCI-EXPANDED)	1975-present	网络版
JCR-(Journal of Citation Report)	2021	网络版
中国科学院文献情报中心期刊分区表（基础版）	2021	网络版

三、检索结果

委托人提供的**1**篇论文被SCI-E收录，论文收录、所在期刊的影响因子及中国科学院文献情报中心期刊分区表情况见附件一。

特此证明！

东北师范大学科技查新咨询中心

教育部科技查新工作站（L24）

（盖 章）

检索报告人：曹宇

2022 年 11 月 14 日

附件一： SCI-E收录情况

第 1 条，共 1 条
标题: Dual hybrid convolutional generative adversarial network for hyperspectral image classification
作者: Shi, CP (Shi, Cuiping); Zhang, TY (Zhang, Tianyu); Liao, DL (Liao, Diling); Jin, Z (Jin, Zhan); Wang, LG (Wang, Liguo)
来源出版物: INTERNATIONAL JOURNAL OF REMOTE SENSING 卷: 43 期: 14 页: 5452-5479 DOI: 10.1080/01431161.2022.2135412 出版年: JUL 18 2022
Web of Science 核心合集中的 "被引频次": 0
被引频次合计: 0
使用次数 (最近 180 天): 0
使用次数 (2013 年至今): 0
引用的参考文献数: 53
摘要: Generative adversarial networks (GANs) have effectively promoted the development of hyperspectral image classification technology in generating samples. Many GAN-based models for hyperspectral image classification use deconvolution to generate fake samples, which will cause chequerboard artefacts and affect classification performance. Furthermore, the training of GANs still faces the problem of mode collapse. Aiming at the above problems, we proposed a dual hybrid convolutional generative adversarial network (DHCGAN) for hyperspectral image classification. Firstly, the combination of nearest neighbour upsampling and sub-pixel convolution is employed in the generator, which avoids the overlap of convolution domain and effectively suppresses the chequerboard artefacts caused by deconvolution. Secondly, the traditional convolution and dilated convolution are fused in the discriminator, which expands the receptive field without increasing parameters and achieves more effective feature extraction. In addition, some adaptive drop blocks are embedded into the generator and discriminator to effectively alleviate the problem of mode collapse. Experiments were performed on four hyperspectral datasets (including three classical datasets - Indian Pines, University of Pavia and Houston, a new dataset - WHU-Hi-HanChuan). Experimental results show that the proposed method can provide a certain performance improvement over some competing methods, such as the accuracy has been increased by more than 1% on the three classical datasets, and even got over 3% improvement on WHU_Hi_HanChaun dataset.
入藏号: WOS:000871760000001
语言: English
文献类型: Article
作者关键词: hyperspectral image (HSI) classification; generative adversarial network (GAN); sub-pixel convolution; hybrid convolution
KeyWords Plus: FRAMEWORK; FUSION
地址: [Shi, Cuiping; Zhang, Tianyu; Liao, Diling; Jin, Zhan] Qiqihar Univ, Coll Elect & Commun Engn, 42 Wenhua St, Qiqihar 161000, Heilongjiang, Peoples R China.
[Wang, Liguo] Dalian Nationalities Univ, Coll Informat & Commun Engn, Dalian, Peoples R China.
通讯作者地址: Shi, CP (通讯作者)， Qiqihar Univ, Coll Elect & Commun Engn, 42 Wenhua St, Qiqihar 161000, Heilongjiang, Peoples R China.
电子邮件地址: shicuiping@qqhru.edu.com
出版商: TAYLOR & FRANCIS LTD
出版商地址: 2-4 PARK SQUARE, MILTON PARK, ABINGDON OR14 4RN, OXON, ENGLAND
Web of Science Index: Science Citation Index Expanded (SCI-EXPANDED)
Web of Science 类别: Remote Sensing; Imaging Science & Photographic Technology
研究方向: Remote Sensing; Imaging Science & Photographic Technology
IDS 号: 5N4KS
ISSN: 0143-1161
eISSN: 1366-5901
29 字符的来源出版物名称缩写: INT J REMOTE SENS
ISO 来源出版物缩写: Int. J. Remote Sens.
来源出版物页码计数: 28
基金资助致谢:
基金资助机构 授权号
National Natural Science Foundation of China
42271409
62071084
Heilongjiang Science Foundation Project of China
LH2021D022
Fundamental Research Funds in Heilongjiang Provincial Universities of China
135509136
This research was funded in part by the National Natural Science Foundation of China (42271409, 62071084), in part by the Heilongjiang Science Foundation Project of China under Grant LH2021D022, and in part by the Fundamental Research Funds in Heilongjiang Provincial Universities of China under Grant 135509136.

输出日期: 2022-11-14

期刊< INTERNATIONAL JOURNAL OF REMOTE SENSING >IF（2021 年）：

INTERNATIONAL JOURNAL OF REMOTE SENSING

期刊影响因子™

2021	五年
3.531	**3.79**

中国科学院文献情报中心期刊分区表（基础版）（2021年）如下：

中国科学院文献情报中心期刊分区表 浏览 检索 批量检索 阈值 公告 升级版 绑定微信 dbsfdx 退出

期刊全称：	INTERNATIONAL JOURNAL OF REMOTE SENSING		
期刊简称：	INT J REMOTE SENS	ISSN：	0143-1161
年份：	2021年	综述：	否

	学科名称	分区	Top期刊
小类	IMAGING SCIENCE & PHOTOGRAPHIC TECHNOLOGY成像科学与照相技术	3	-
小类	REMOTE SENSING遥感	4	-
大类	工程技术	3	否

The End